

Cs₂AgBiBr₆ Double Perovskites as Lead-Free Alternatives for Perovskite Solar Cells?

Wolfgang Tress* and Maximilian T. Sirtl

Finding lead-free alternatives remains an important and challenging topic in the field of perovskite solar cells. In this perspective, the potential of Cs₂AgBiBr₆ double perovskites in solar cells is discussed based on reported absorption and emission data. Whereas the material is capable of exceeding and potentially doubling current efficiency values of around 3%, mainly by an optimized solar cell design, industrially relevant devices cannot be fabricated without major changes in the absorption onset. Nevertheless, Cs₂AgBiBr₆ poses various scientific questions and exact recombination and charge transport processes are yet to be unraveled, preparing us for the double perovskite or perovskite-like materials to come.

environment compared to lead emission from other sources,^[3] there is a high urge to replace Pb or find similar lead-free materials, which maintain the excellent optoelectronic properties of the lead-halide perovskites. This is a challenging endeavor as various criteria must be fulfilled: the material should form a stable perovskite phase, can be deposited as a thin film, should have a suitable bandgap, provide mobile nonbound charge carriers, and show a high defect tolerance. The most straightforward approach toward eliminating Pb is to replace the Pb in the A⁺Pb²⁺X₃⁻ com-

compound by another divalent cation such as Ge or Sn while maintaining the metal-halide perovskite structure.^[4] Sn-based perovskite solar cells have been realized and seen continuous improvement.^[5–7] However, a large number of defects challenge their application as an efficient photovoltaic material. Furthermore, the stability of the perovskite compound with Sn²⁺ readily oxidizing to Sn⁴⁺^[8] supercharges the encapsulation demands, which are already challenging for the lead perovskites.

To widen the choice of possible perovskite compounds, one can spread toward double perovskites. In such compounds, the Pb site is replaced alternately by cations with formal oxidation state +1 and +3 ions, the most prominent being Cs₂AgBiBr₆ (Figure 1).^[9,10] Single crystals,^[9,11,12] thin films, and solar cells^[13–16] have been realized within the past 5 years. However, the PCE remained just above 3% for single-junction solar cells despite a considerable effort in characterizing the material and engineering the devices. Beyond these low PCE values, the absorption and emission features of Cs₂AgBiBr₆ pose various unanswered questions and lead to very different interpretations on bottlenecks and the theoretical potential of this material.

In this perspective, we want to discuss reported experimental observations from the solar cell physicist's point of view. We do not intend to provide a comprehensive review on the material, which can be found elsewhere.^[17–19] Instead, we will sort the reported results and present a theoretical efficiency estimate based on measurement data without extrapolations to bandgaps. We will discuss major bottlenecks, also by comparing to lead-halide perovskites and report approaches to reduce them. Furthermore, we will add points, which we see as unresolved questions and trajectories toward more efficient solar cells.

1. Introduction

Lead-based perovskites are outstanding semiconductors and comprise almost all features required for sustainable thin-film photovoltaics.^[1,2] The solar cells can be fabricated by low-cost low-temperature solution processing technologies and precursor materials do not involve energy-intensive purification. Furthermore, no scarce elements are required and the thin active layer, half a micron thick, minimizes material consumption. Therefore, in the order of 1 g absorber material is needed for a square meter of module. At the same time, power conversion efficiencies (PCEs) exceeded 25% on lab scale devices and it is a matter of a few years until perovskite modules with PCEs similar to those of silicon will be available.


However, there is one major drawback. The material contains the heavy metal lead, which is toxic and its use in electronics is restricted in many regions of the world. This disadvantage is even more problematic as the perovskite is water soluble. Despite the discussions on whether the little amounts of lead in perovskite modules constitute a tolerable risk of contamination of the

W. Tress

Novel Semiconductor Devices Group, Institute of Computational Physics
Zurich University of Applied Sciences
Wildbachstr. 21, 8401 Winterthur, Switzerland
E-mail: wolfgang.tress@zhaw.ch

M. T. Sirtl

Department of Chemistry and Center for NanoScience (CeNS)
University of Munich (LMU)
Butenandtstr. 11, 81377 Munich, Germany

 The ORCID identification number(s) for the author(s) of this article can be found under <https://doi.org/10.1002/solr.202100770>.

© 2021 The Authors. Solar RRL published by Wiley-VCH GmbH. This is an open access article under the terms of the Creative Commons Attribution License, which permits use, distribution and reproduction in any medium, provided the original work is properly cited.

DOI: 10.1002/solr.202100770

2. The Bandgap and the Maximum Photocurrent

The bandgap E_g is the most important material property for a solar cell's absorber. Using the framework developed by

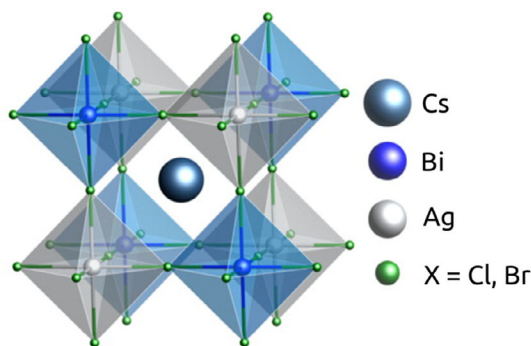


Figure 1. Double perovskite structure. Reproduced with permission.^[35] Copyright 2016, American Chemical Society.

Shockley and Queisser, one can directly predict the maximum efficiency of a terrestrial solar cell as a function of E_g , the so-called Shockley–Queisser (SQ) limit, as shown in **Figure 2a**. Thus, precisely knowing E_g is essential. The SQ limit assumes a Heaviside function for the absorption, meaning that all the incident light with energy larger than E_g is absorbed and converted to electrical current. However, in real materials, the absorption onset is not that sharp and especially if the layer cannot be made sufficiently thick, the transmission of photons with energies above E_g is not negligible. Also in such cases, a value for E_g can be determined from absorption measurements, e.g., using the Tauc method, which allows to extrapolate to E_g if the nature of the transition at the bandgap (direct/indirect) is known. For $\text{Cs}_2\text{AgBiBr}_6$, various E_g (indirect) values have been reported for the absorption onset, spanning from 1.95 eV^[9] (1.83 eV with phonon absorption), to 2.19 eV^[10] to 2.25 eV,^[20] although considerable absorption is mostly seen below 500 nm (>2.5 eV), close to the direct bandgap. Based on the SQ formalism, these values would allow for theoretical photocurrents and PCEs between 17 mA cm⁻², 25% (for 1.9 eV) and 6 mA cm⁻², 12% (for 2.5 eV), as visualized by the shaded area in **Figure 2a**. These values are very different from a calculated spectroscopic limited maximum efficiency (SLME) of 7.9%,^[21] which based on first-principle calculations takes into account the calculated shape of the absorption spectrum and nonradiative recombination.^[22]

This wide spread in E_g concomitant with promising PCE values makes us examine measured absorption spectra. Selected literature data are shown in **Figure 3**, revealing two striking features: first, the shape does not look like what is expected for a band edge absorber with a E_g around 2 eV (600 nm), which is in contrast to lead-based perovskites. Instead, the material shows weak absorption in this range and several features for higher energies. Second, the spectra vary considerably. This is in strong contrast to lead-based perovskites, where a reproducible bandgap can be seen, which can be tuned by the halide composition (see, e.g., the absorption of $\text{FAPbI}_y\text{Br}_{1-y}$ in ref. [23]). Obviously, the fabricated films are not identical and other effects play a role such as impurity phases or a dependence on the orientation of grains in the film. Even a recent study demonstrated that the absorbance of films obtained by different synthesis methods varies and does not simply scale as expected from the film thickness (**Figure 3a**).^[24] Nevertheless, most spectra have the following in common: high absorption below 340 nm (3.6 eV), a strong feature at around 440 nm (2.8 eV), and weak absorption at lower energy, where the indirect bandgap is expected, although the signal at the indirect gap (650 nm, 1.9 eV) is weak and only determined by extrapolation in the mentioned Tauc plots. Furthermore, there is a tail toward even lower energies which seems to be more or less pronounced but contributed to photocurrent in the solar cells presented in the study by Gao et al.^[14] (**Figure 3e**). We will discuss the absorption features in more detail later and continue with an estimation of the maximum photocurrent based on the absorption data itself.

Given these absorbance spectra, one can go another way to determine the maximum photocurrent than extrapolating to the bandgaps. Instead, one calculates the absorption (details regarding approximations in Supporting Information) and estimates the number of harvested photons from the solar spectrum. The result for the film with antisolvent of **Figure 3a** is illustrated in **Figure 2b**, which shows the solar spectrum and the harvested spectral photon flux, which integrates to 5 mA cm⁻² electrical current density, similar to what has been stated in the study by Ning et al.^[25] It is obvious that the (120 nm) layer is not sufficiently thick to absorb a considerable share of solar photons with wavelength above 450 nm (2.75 eV). At 1.9 eV (650 nm), the (lower estimate for the) indirect E_g , the harvested photon flux approaches zero.

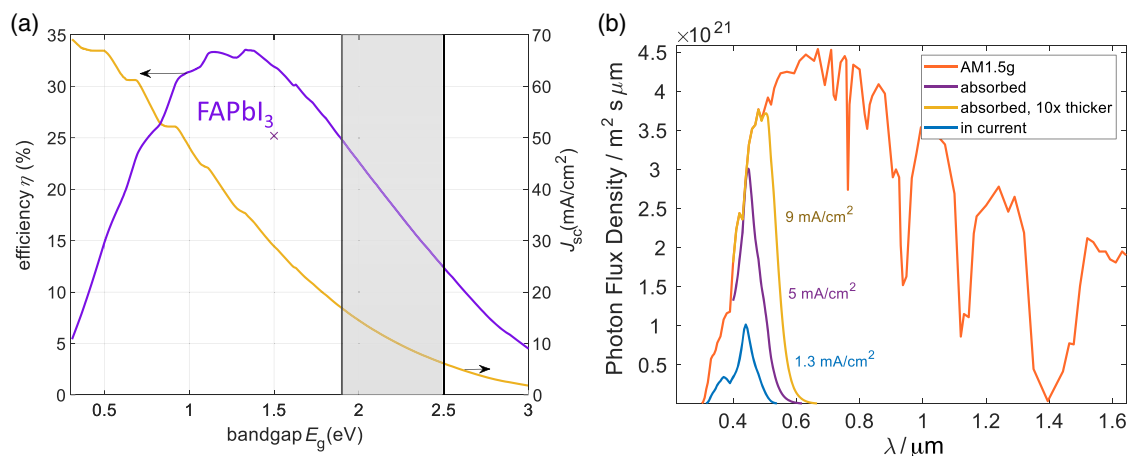


Figure 2. Limits. a) SQ limit for efficiency (blue) and photocurrent (yellow). b) Absorbed photon flux density from AM1.5g and maximum photocurrent calculated from device data of Sirtl et al.^[24] (EQE in **Figure 3d**).

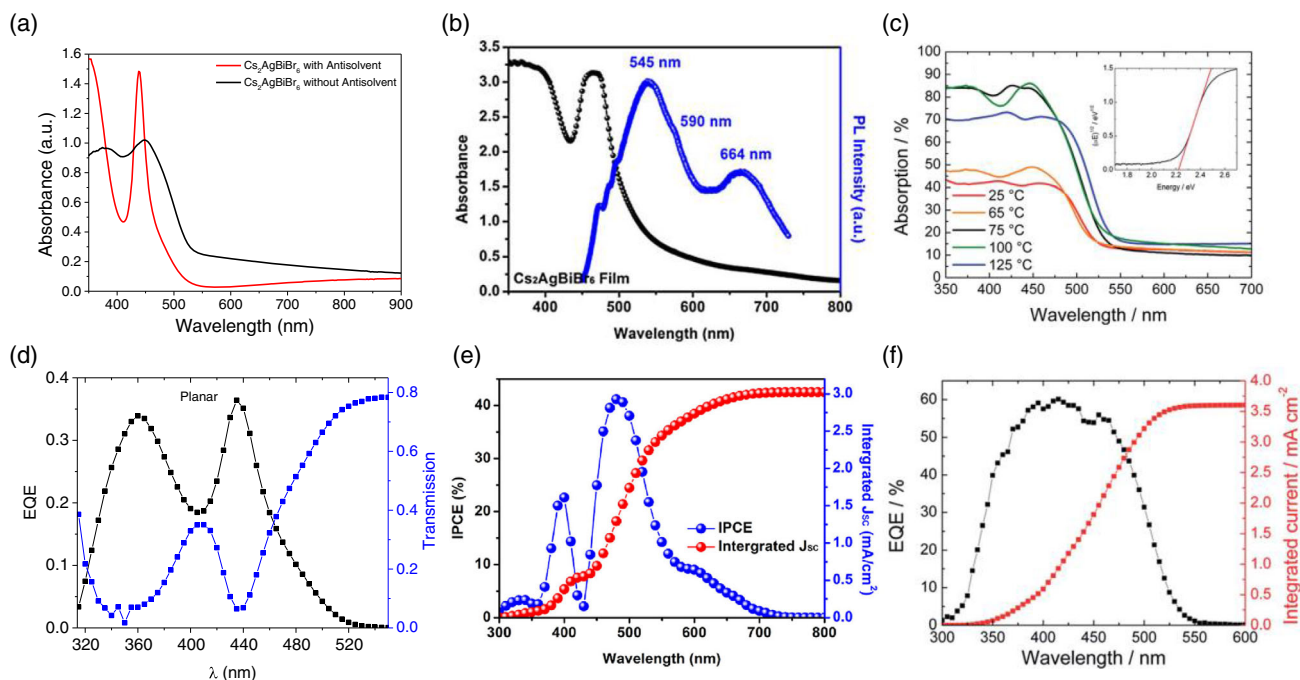


Figure 3. Absorption and external quantum efficiency (EQE) spectra of $\text{Cs}_2\text{AgBiBr}_6$ films used in solar cells. a) Absorbance of two films obtained by different methods. Reproduced under the terms of the CC-BY-NC license.^[24] Copyright 2021, The Authors. *Advanced Optical Materials* published by Wiley-VCH GmbH. b) Absorbance and PL of films. Reproduced with permission.^[14] Copyright 2018, Wiley-VCH. c) Absorption of films as a function of preheating temperature. Reproduced with permission.^[13] Copyright 2017, The Royal Society of Chemistry. d) EQE compared with transmission for solar cells with the antisolvent film from (a). Reproduced under the terms of the CC-BY-NC license.^[24] Copyright 2021, The Authors. *Advanced Optical Materials* published by Wiley-VCH GmbH. e) EQE and integrated current for devices made with film from (b) and f) from (c). e) Reproduced with permission.^[14] Copyright 2018, Wiley-VCH. f) Reproduced with permission.^[13] Copyright 2017, The Royal Society of Chemistry.

Assuming that the layer was ten times optically thicker (which could be achieved by increased layer thickness, a reflector, or light trapping schemes), the achievable current would increase up to 9 mA cm^{-2} , which we want to state as a pragmatic maximum. This value is almost half compared to the one of a band edge absorber at 1.9 eV (Figure 2a). Measured currents of 1.3 mA cm^{-2} for planar cells^[26] and $4\text{--}5 \text{ mA cm}^{-2}$ for mesoporous TiO_2 -based ones^[13,16] could not reach this value yet.

3. Luminescence and Voltage

The SQ limit assumes an ideal absorber embedded between ideal contacts, meaning that all recombination is radiative, emitting photons with an energy narrowly distributed around E_g . In such a case, the theoretical maximum open-circuit voltage V_{oc} can be reached. Thus, it is essential to know the luminescence properties of $\text{Cs}_2\text{AgBiBr}_6$. It was found that the photoluminescence (PL) yield of the material is in a promising range (0.01% for an excitation density comparable to 1 sun ^[27] or 0.08% in another study^[28]) and that the PL decay is rather slow (200 ns in a film,^[13] $>500 \text{ ns}$ in single crystal,^[9] details later). The latter indicates long-living charges, an early finding that stimulated the interest in the research community.^[9] However, the PL spectrum is significantly redshifted compared to the absorption (Figure 4a). Furthermore, the electroluminescence (EL), measured at devices and ideally directly related to V_{oc} through an optoelectronic reciprocity relation,^[29] is even further redshifted (green curve in

Figure 4a). Therefore, it is not straightforward to predict a V_{oc} limit. However, the external yield of the EL, which is measured to 10^{-8} in a device that showed a voltage of $\approx 1.0 \text{ V}$, results in a V_{oc} loss due to nonradiative recombination of $\approx 0.5 \text{ V}$. The difference of the EL yield compared to the PL yield can be attributed to recombination at the contacts, which will be discussed with other bottlenecks after we had a more detailed look at the absorption and emission spectra.

4. Absorption Onset and Emission in More Detail

To determine the radiative V_{oc} limit based on detailed balance, the absorption onset is important. In the more general reciprocity relations,^[29] one can also use the spectral photocurrent response, which can be very accurately measured. Figure 4b from Sirtl et al.^[24] shows an example. The above-gap features reproduce the absorption, accompanied by a broad onset distinct above 2 eV and by further tail states at lower energies. The origin of these deep states is unclear and they cannot be considered when calculating the radiative V_{oc} . Otherwise, V_{oc} would be unrealistically low. Consequently, these tails are not in equilibrium with free charges that generate V_{oc} . However, the broad absorption onset is consistent with the shifted PL and results in a radiative V_{oc} of 1.94 V .^[24] Therefore, the shifted and broad PL does not urge for an additional emissive state in the bandgap but is sufficiently well explained by the broad absorption onset. The reason for the broad onset could be disorder in the material, e.g., related to nonhomogeneously alternating B site occupation by Ag and Bi

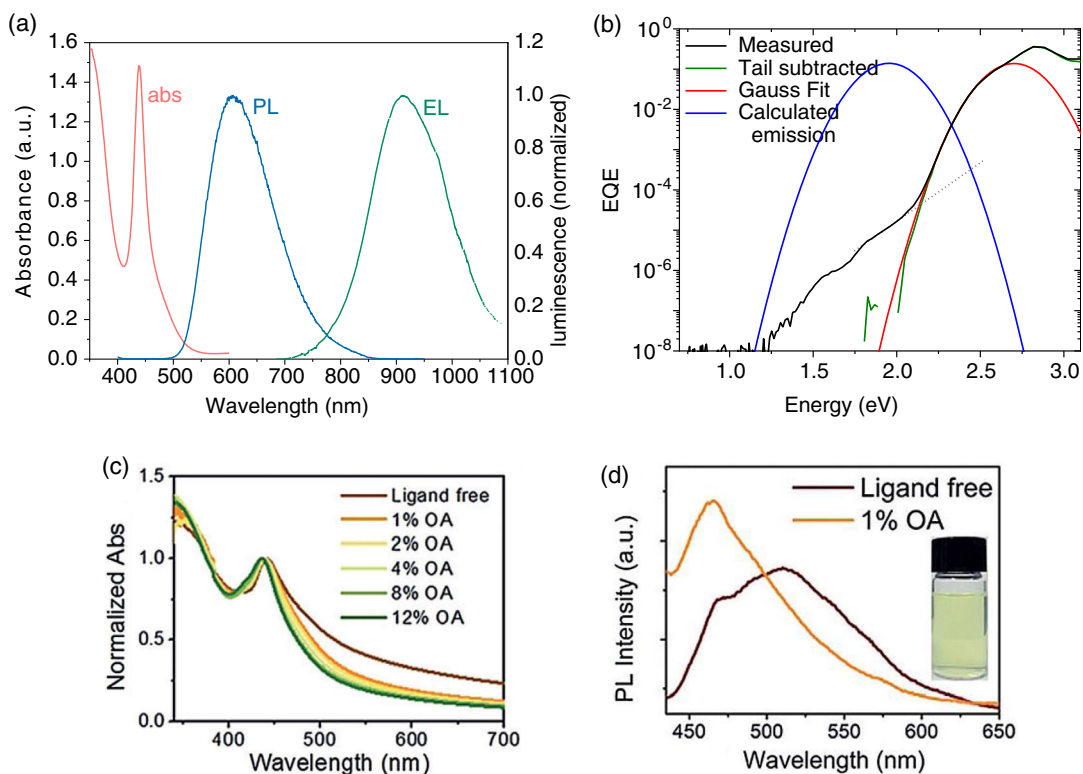


Figure 4. Absorption and emission in detail. a) Absorption, PL, and EL of $\text{Cs}_2\text{AgBiBr}_6$ thin films and devices. b) Sensitive measurement of the EQE. Reproduced under the terms of the CC-BY-NC license.^[24] Copyright 2021, The Authors. *Advanced Optical Materials* published by Wiley-VCH GmbH. c) Absorption and d) PL of $\text{Cs}_2\text{AgBiBr}_6$ nanocrystals as an example where the PL is much less shifted than in most of the reported films and single crystals. Reproduced with permission.^[34] Copyright 2018, Wiley-VCH.

as predicted from a first principle study, where the calculated E_g can be decreased down to 0.5 eV.^[30] Other proposed reasons for the large Stokes shift are strong electron–phonon Fröhlich interactions^[31] leading to a self-trapped exciton,^[32] or an emissive color center^[33] based on PL excitation (PLE) spectra despite the fact that the PLE in other studies expectedly follows the absorbance.^[28]

Whereas the broad shifted PL in Figure 4a is rather representative (modified by slight changes in the maximum between 500 and 600 nm, also possibly showing a more structured shape as in Figure 3b) for the emission of films and single crystals, nanocrystals seem to be an exception, where the PL spans the absorption range and peaks at 460 nm (Figure 4c,d).^[34]

5. Absorption Features and Emission Lifetimes

Interestingly, the different absorption features are 1:1 visible in the EQE (Figure 3d), meaning that charge separation and collection does not depend on the specific absorption mechanism. Nevertheless, it is interesting to briefly summarize the explanations given in the literature for the absorption features.

As already mentioned, the broad onset is attributed to transitions close to the indirect bandgap (Tauc extrapolated 1.9 eV), which explains the weak signal. The absorption at 440 nm (2.8 eV), which is often seen as a prominent peak, is mostly related to the direct bandgap (>2.2 eV in Tauc analyses^[9]).

This is roughly consistent with DFT calculations^[35] predicting an indirect gap at 1.8 eV and a direct one at 2.5 eV.

In a detailed study,^[32] the peak at 440 nm is suggested to be excitonic (bound direct-gap electron–hole pair), and the higher energy signal peaking below 400 nm resulting from direct band-to-band transitions. The direct bandgap is then 387 nm (3.20 eV), derived by a Tauc analysis and considering the exciton via the Elliot equation. The exciton binding energy is determined to 268 meV.^[32] This value is much larger than what is reported for lead-halide perovskites and in a range, more common for organic semiconductors, where such excitons do not split instantaneously at room temperature. One important material parameter, determining the exciton binding energy in a simple Coulomb model, is the static dielectric constant of the surrounding ϵ_r , which is 3–5 for organics and 30 for MAPbI_3 .^[36] For $\text{Cs}_2\text{AgBiBr}_6$, a value of 21 is determined from impedance spectroscopy (own measurements) (16.7 from density functional perturbation theory^[31]), which would result in a (Wannier–Mott) exciton binding energy $E = \frac{m_e^* m_h^*}{m_e^* + m_h^*} \frac{Ry}{m_0 \epsilon_r^2}$ in the 3–5 meV range, considering the effective electron and hole masses (m_e^* , m_h^*) of 0.37 and 0.14 free electron masses m_0 .^[10]

An alternative explanation has been proposed based on temperature-dependent investigations of the absorption. There it was found that the 440 nm peak does not shift as the bandgap does, which is seen as evidence for a nonexcitonic nature of this state.^[37] Instead, it is regarded as a resonant feature resulting

from local transitions of the Bi^{3+} ion, whose energy (usually $>10\text{ eV}$) might be shifted into this range by the polarizability of the surroundings. Similarly, such intraatomic localized transitions between Bi-s and Bi-p states were proposed in the study by Bekenstein et al.^[38] In that study, interestingly, the signal at 440 nm is discussed from another perspective because nanocrystals have been investigated. The 440 nm peak is compared to the indirect gap, which is around 1 eV lower in energy. Thus, an explanation for the increase in energy would require a quantum-confined exciton, which the authors exclude in favor of the intra-atomic transitions.

It remains interesting why the 440 nm peak depends so much on the film processing as shown in Figure 3a, where both peaks (also the 350 nm) seem to be similarly affected maybe arguing more for a common or correlated origin. Interestingly, also the high-energy absorption results in a rather narrow band as seen from an increase in transmission below 350 nm (Figure 3d).

Already in the first reports, a slow transient PL decay has been found, on both powders and crystals (Figure 5a) and later on thin films as well (Figure 5b,c). Whereas a long PL lifetime is commonly desired as it implies slow nonradiative recombination, the situation for $\text{Cs}_2\text{AgBiBr}_6$ is more complex, also due to the strongly shifted PL. Therefore, the decay time in the 100 s of ns, which would indicate high-quality films in the case of lead-halide perovskites, does probably not describe the lifetime of free carriers in $\text{Cs}_2\text{AgBiBr}_6$. In fact, only a small fraction of the PL intensity decays that slowly. The largest fraction decays within a couple of ns (marked in the plots of Figure 5). This decay might represent the lifetime of charge carriers, which is actually low, e.g., due to fast recombination or trapping. The longer-lived component might result from detrapping of charges in shallow states.^[39] An interesting observation was made in transient absorption (TA) spectroscopy, where a photoinduced absorption signal was detected that emerged during the PL decay in the first 100 ns after the light pulse and persisted for more than a μs .^[27] From this, a “fundamental carrier lifetime” $>1\ \mu\text{s}$ was claimed, very high charge carrier densities under solar illumination calculated, and concluded that charge-transport properties are sufficient to allow for thicker films.^[27] However, PL remains the measurement of choice for measuring the majority of free carriers and the TA signal, which spectrally coincided with the PL, might be interpreted differently.

6. Doubling the Efficiency from 3% to 6%: Device Optimization—Charge Transport and Extraction

Now we want to come back to the reasons for the low device performance. Investigating the reported solar cell data, one can conclude that the following processes are not the major efficiency bottleneck. 1) Separation of charge carriers or splitting of excitons. Such processes usually result in enhanced photocurrents under reverse bias and might lead to different signatures for free charges and excitons in the spectral response. Such effects have not been observed. 2) Intrinsic transport of charges. The PL is strongly quenched in devices compared to films,^[24,40] indicating that charges indeed reach the adjacent layers and recombine there nonradiatively. Also applying a certain prebias allows for much higher currents under a fast J - V scan, indicating that indeed drift mobilities are sufficient.^[24] Diffusion lengths of excited species without discrimination (excitons, electrons, holes?) have been estimated to 100 nm by a PL quenching experiment on films.^[25] An ambipolar diffusion length of $>1\ \mu\text{m}$ was reported for single crystals using stroboscopic scattering microscopy.^[41] Such values translate in decent mobilities. In time-resolved microwave conductivity (TRMC), $>1\ \text{cm}^2\text{Vs}^{-1}$ ^[42] and up to $5\ \text{cm}^2\text{Vs}^{-1}$ ^[26] have been reported, which is just one order of magnitude lower than for lead-based perovskites. Despite the shallow traps, a band-like transport was deduced from TRMC,^[43] whereas in another study fast relaxation (1 ps) into a localized state with thermally activated transport has been observed.^[44] Nevertheless, the mobility of this self-trapped excitonic polaronic state is still $1\ \text{cm}^2\text{Vs}^{-1}$, which should allow for sufficient collection of charge carriers. On the other hand, the same authors reported an electron diffusion length of only 30 nm.^[28] Both values combined yield a lifetime of 0.3 ns, which is much lower than seen in PL and might ask for a unified picture. Regarding the p- or n-type behavior there are different findings, mainly advocating for p-type,^[11] which might lead to collection problems of electrons in solar cells.^[28] On the other hand, n-type behavior has been found by photoelectron spectroscopy measurements on single crystals.^[45] To explain higher internal quantum efficiencies for light absorbed closer to the n-contact,^[24,28] low electron diffusion length/mobility, or the mentioned high p-type doping could be an explanation at first glance. However, these

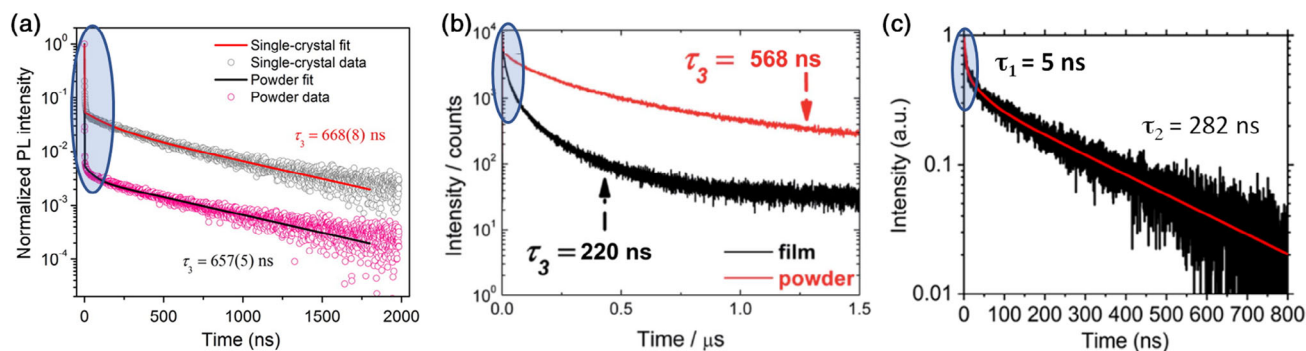


Figure 5. Transient PL. a) Adapted with permission.^[9] Copyright 2016, American Chemical Society. b) Adapted with permission.^[13] Copyright 2017, The Royal Society of Chemistry. c) Adapted with permission.^[46] Copyright 2018, American Chemical Society. In all measurements, a fast initial drop is observable (marked).

explanations are not consistent with a photocurrent (internal quantum efficiency [IQE]) that hardly depends on voltage, the decent fill factors (FFs), and strong luminescence quenching in devices. At the same time, the scan rate-dependent photocurrents^[24] (Figure 6a) show that the electric field has an influence on charge collection, ruling out loss mechanisms based on excitons or photovoltaically completely inactive regions due to isolated grains, etc. Simulated J - V curves in Figure 6b visualize that any transport-limited process of free charge carriers would result in a low FF and eventually higher photocurrent under reverse bias (blue), which is not observed in experiment, demanding for further investigations.

The major bottlenecks that limit the efficiency below 3% seem more related to the contacts. They seem neither optimum for efficient charge collection nor for providing high charge selectivity, as voltage-dependent EQE spectra show.^[24] Changing the hole transport layer (HTL) has indeed been shown to influence the performance and V_{oc} ,^[46] not scaling with the energy levels but obviously influencing surface recombination and selectivity. Solar cells with 1% efficiency discriminate themselves from devices with 2.x% mainly by a higher EQE and internal QE, whereas FF and V_{oc} remain rather unchanged. Generally, using a mesoporous TiO_2 allows for higher currents, which is consistent with the finding of limited charge collection further away from the n-contact.^[24] The scan rate-dependent photocurrents (Figure 6a) indicate that the interplay between charge collection and recombination at the contacts is influenced by a slow processes, possibly related to mobile ions,^[47] which have been observed^[11,48] in the material but not yet investigated in detail. Those ionic charges could explain the low but voltage-independent IQE (i.e., decent FF > 70%, especially for planar devices^[24]). Therefore, engineering the contacts toward highest selectivity and aligned energy levels will be required to enhance the PCE. However, to achieve phase purity and to prevent the formation of undesired secondary phases such as $Cs_2Bi_3Br_9$ or $AgBr$, high annealing temperatures of over 250 °C are necessary.^[13] Hence, testing alternative substrates and underlying charge

transport layers is hardly feasible as it was shown that, e.g., the Fermi level of ALD-processed SnO_x electron-transport layer (ETL) is strongly dependent on the annealing temperature.^[49]

Figure 7 shows a rough estimation of what could be gained, when certain processes are optimized. Enhancing the IQE (charge collection) of our 1% reference device and optimizing the thickness would allow to reach 5% PCE. Making the photocurrent less dependent on the voltage to enhance the FF toward 75% would give $\approx 6\%$. Enhancing the EQE EL by enhancing the contact selectivity toward the best PL yield (0.1%) would give a V_{oc} boost of 0.3 V and even further enhancing the PL yield would allow the PCE reaching 10%. Only if it was possible to avoid the redshifted EL and broad PL, the V_{oc} could be further enhanced to reach the SQ limit of 16% (based on 9 mA cm^{-2}), which also requires a FF > 90%. However, the PL as discussed above seems to be a very reproducible property of $Cs_2AgBiBr_6$ thin films, whose origin remains under debate.

7. The Role of Fabrication Methods

Although films of different fabrication methods qualitatively share the major optoelectronic properties such as the absorption and broad PL features (as expected for nominally the same material), further properties such as luminescence yields, film morphology, and solar cell efficiency vary considerably with deposition method. This becomes obvious from research in the last years, reporting a large variety of synthesis and deposition methods in order to control crystallinity, orientation of the thin films, as well as the optoelectronic behavior of both thin films and single crystals. For single crystals, the mostly used synthesis method is the slow cooling method from the hot acidic solution with approximately $0.5\text{--}2 \text{ }^\circ\text{C h}^{-1}$ cooldown rate.^[9,50–52] In order to change the ordering and/or the crystallinity, several methods have been applied including washing the crystal with 2-propanol or ethyl acetate, as well as adding small amounts of phenethylammonium bromide.^[11,53] The treatment with

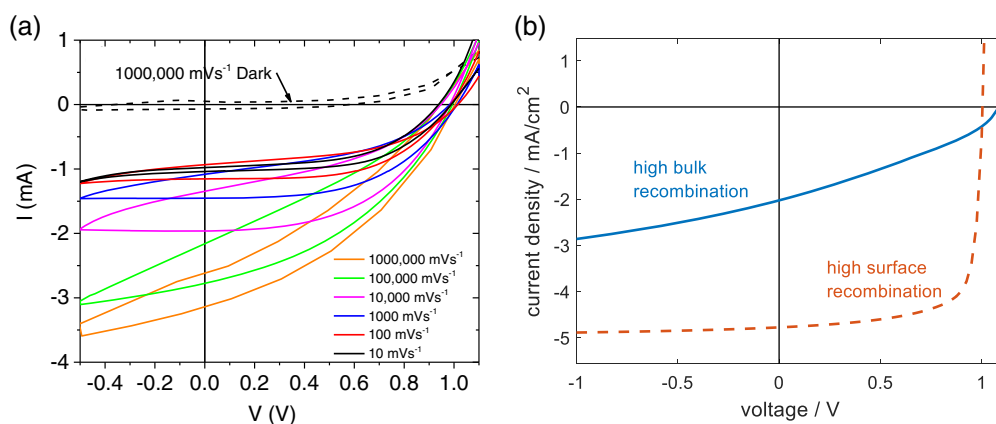


Figure 6. J - V curves. a) Measured data under various scan rates after positive prebias. Reproduced under the terms of the CC-BY-NC license.^[24] Copyright 2021, The Authors. *Advanced Optical Materials* published by Wiley-VCH GmbH. b) Simulated J - V curves for a 120 nm-thick active layer with a bandgap of 2 eV and electron and hole mobility of $1 \text{ cm}^2 \text{ Vs}^{-1}$. The blue curve assumes that Shockley-Read-Hall (SRH) recombination limits the V_{oc} . A low IQE of 40% at short circuit is accompanied by a low FF of 32%. The red dashed curve shows an example where the work functions of nonselective contacts (built-in potential = 1.2 V) limit V_{oc} . The FF reaches 75%. The red curve is closer to what is seen in experiment. However, only except for an additional voltage-independent photocurrent loss, whose origin is waiting for a detailed explanation. Details regarding the simulations in Supporting Information.

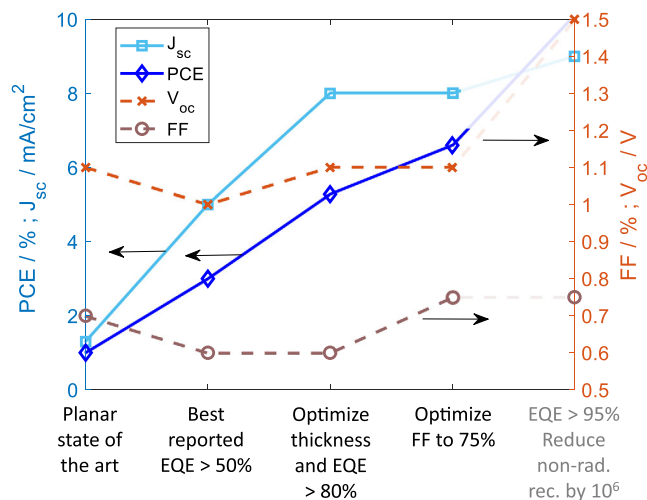


Figure 7. Optimistic PCE trajectory. Optimizing charge collection by engineering the device architecture could double the PCE from 3% to 6%. Approaching 10% will only be possible if nonradiative recombination at the contacts and in the absorber is strongly reduced.

isopropanol, together with thermal annealing at 100 °C, led to a blueshift of the PL signal from 634 to 593 nm with a reduced full width at half maximum (FWHM) which was linked to a reduction of the trap density in the single crystal.^[11] Another recently published work used a slow evaporation method using dimethyl sulfoxide (DMSO) and DMSO/dimethylformamide (DMF) blends as solvents, leading to single crystals that reveal film-like optoelectronic properties as shown by PLE measurements.^[12]

Thin film synthesis, however, encounters several issues regarding crystallinity and phase purity. To ensure that no precursor traces or secondary phases such as Cs₃Bi₂Br₉ or Cs₂AgBr or Cs₃AgBr₂ are present in the thin films, postannealing of at least 250 °C has to be applied. While the annealing temperature can be slightly reduced to 200 °C by vacuum-assisted annealing beforehand,^[54] other techniques such as laser assisted (at 200 °C process temperature),^[55] spray coating,^[56] and vapor-assisted deposition^[15,28,57–59] demand for high annealing temperatures and yield power conversion efficiencies of only up to 1.41% in solar cells. The most commonly used technique, however, is spin coating during which the double perovskite solution (usually with concentrations of 0.5–0.6 M) is dropped quickly on a fast-spinning substrate. To improve the crystallization and the film morphology, a second step can be performed, during which an antisolvent (solvent in which the double perovskite is poorly to nonsoluble) is added to both initiate a fast crystallization and wash out the perovskite solvent. While the use of an antisolvent drastically improves the film morphology (more conformal films, **Figure 8**), the result is highly influenced by the speed of addition, the duration of the addition, and the antisolvent itself.^[60] Moreover, thin films synthesized with an antisolvent are commonly thinner compared to films formed without antisolvent which is a drawback considering the weak absorption due to the indirect bandgap of the material.^[24]

To achieve a high crystallite orientation, as well as a rather high crystallinity of the thin films, either complicated syntheses

have to be used, or the presence of (nondetrimental) secondary phases has to be accepted.^[26,45] Also, additive addition has proven to improve the thin film crystallinity.^[61–63] The highest PCE using an antisolvent was achieved by Gao et al. for a planar heterojunction in n–i–p architecture.^[14] Yet, the highest efficiencies have been achieved without antisolvent, using either a mesoporous or compact TiO₂ scaffold as ETL.^[15] The highest PCEs for solar cells comprising pure Cs₂AgBiBr₆ were obtained modifying both hole-transport material (HTM) and ETL in order to improve the energy-level alignment,^[64] as well as the charge carrier extraction.^[16]

While the stoichiometric ratios of the elements were discussed to influence the solar cell performance,^[15,26] theoretical predictions regarding its effect on the optoelectronic properties do not provide a consistent picture. In one study, it was suggested that Br-poor/Bi-rich conditions could enhance performance (due to bismuth vacancies (V_{Bi}) and silver/bismuth antisite defects (Ag_{Bi}) forming deep acceptor levels).^[65] In another study, bismuth/silver antisite defects (Bi_{Ag}) and bromine vacancies (V_{Br}) have been identified as deep electron traps with low formation energies and therefore Bi-poor/Br-rich conditions would be desired^[66] which could be confirmed experimentally in slightly enhanced luminescence yields and PCEs.^[26] While controlling the stoichiometry of the Cs₂AgBiBr₆ precursors did show improved reproducibility, as well as solar cell performance, it was also assigned to the control of the growth conditions in order to increase the film orientation,^[26] similar to lead-based perovskites. However, the effects did not prove to be significant as PCEs >3 % have not been realized.

8. Going Further—Open Questions

Efficiency targets below 10% are not interesting for single-junction solar cell applications. Similar to the pure Br lead halide perovskites, the E_g is too high and photocurrents are too low, also for employment in multijunction cells. Therefore, given the reported absorbance data and realistic layer thicknesses, Cs₂AgBiBr₆ is neither suitable for a tandem with silicon nor for a quadruple junction where $\approx 10 \text{ mA cm}^{-2}$ (and of course a voltage considerably larger than 1.2 V) would be required for the highest-gap sub-cell.

8.1. Further Applications

Working on the device architecture (contact layers, film optimization, etc.) as discussed in the previous section will help to eventually reach $V_{oc} > 1.2 \text{ V}$ and higher IQEs. Especially the energy-level alignment of the valence band maximum toward the HTM gives large room for improvements. Understanding the bottlenecks of double perovskite solar cells will be beneficial for similar materials, given the rather unique physical and chemical properties. However, while it should lead to a maybe double efficiency of the state-of-the-art PCE, working on the device architecture will not help to overcome the hampering factors regarding industrial solar cell applications. Yet, combination with other absorbers is possible^[67] and further applications have attracted a lot of interests. Photodetectors in the blue and UV region in solar cell architecture and as photoconductors were synthesized using

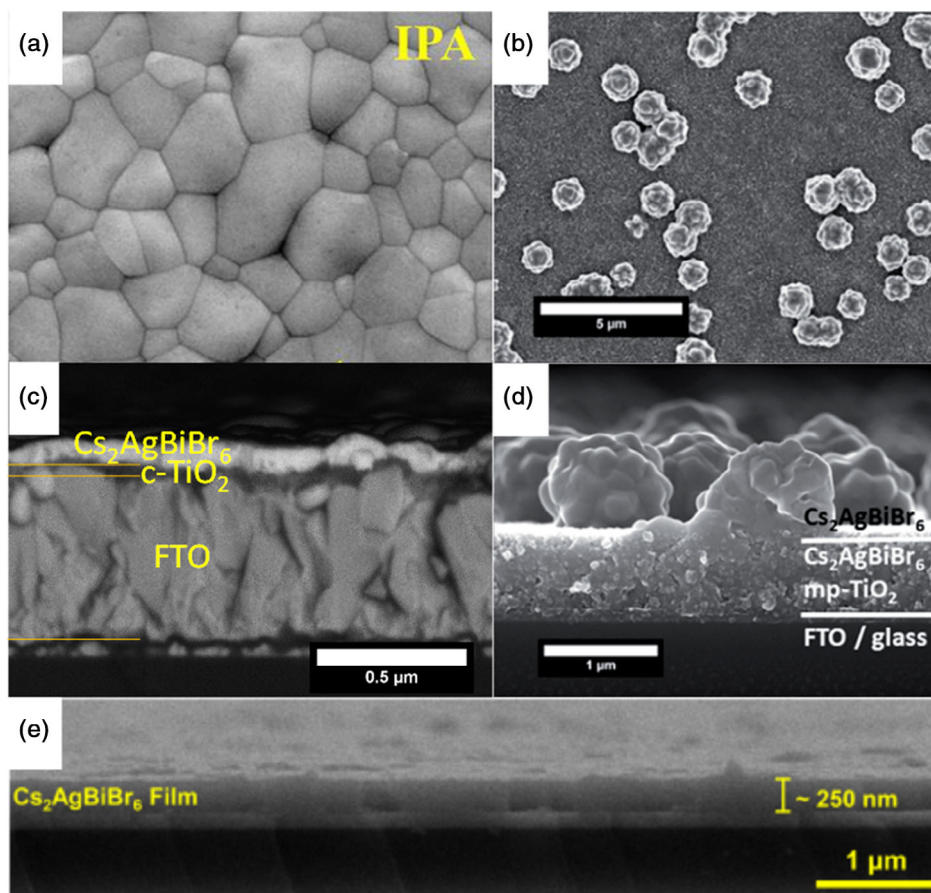


Figure 8. Morphology of $\text{Cs}_2\text{AgBiBr}_6$ thin films. a,c,e) scanning electron microscope (SEM) top views and cross sections for films with antisolvent and b, d) without antisolvent on mesoporous TiO_2 . a,e) Reproduced with permission.^[14] Copyright 2018, Wiley-VCH. b,d) Reproduced with permission.^[13] Copyright 2017, The Royal Society of Chemistry.

various techniques and have proven to be highly responsive with fast response times and detectivity values superior to lead-based perovskites while maintaining the high stability of the material itself.^[57,68–72] Moreover, the application for X-ray detection was investigated in single crystals,^[11,51,53] with promising detection limits, where it was shown that modest cooling during synthesis improves the sensitivity of the single crystal.^[50] While single crystals were in the main focus of research regarding X-ray detection, thin films and even flexible substrates have been realized as well.

8.2. Lowering the Bandgap

For solar cell applications, a lower bandgap is required. Thus, a 3D iodine or mixed I:Br compound would be the breakthrough as the bandgap is expected to be significantly lower. For $\text{Cs}_2\text{AgBiI}_6$, the indirect gap is calculated to 1.08 eV and the direct to 1.79 eV.^[21] However, so far no synthesis route of those 3D compounds has been found and they are thermodynamically unstable.^[21] For example, formation via anion exchange has not been realized in crystals nor in thin films because of the low thermodynamic stability of $\text{Cs}_2\text{AgBiI}_6$.^[73] While this material readily forms the ternary compound $\text{Cs}_3\text{Bi}_2\text{I}_9$, which has been investigated in the community already and expresses poor optoelectronic and photovoltaic properties,^[74] the quarternary structure

of $\text{Cs}_2\text{AgBiI}_6$ can only be stabilized in nanocrystals after complicated anion exchange procedures with methylsilane compounds.^[75,76] A promising procedure to stabilize the iodine perovskite was initially shown by the Mitzi group, where large cations have been implemented in the perovskite structure to form a 2D compound.^[77] Here, (bisaminothyl)bithiophene was implemented to form $(\text{AET})_2\text{AgBiI}_8$ which shows a drastic change in the bandgap by means of energy reduction (2.0 eV) and nature (transition from indirect to direct) which was then realized by other groups using different spacer cations.^[78,79] While pure 2D perovskites are known to have reduced charge carrier mobility and, ultimately, lower PCE in photovoltaic devices, they open up a pathway to chemically not only reduce the bandgap (when the Br content is reduced) compared to the 3D $\text{Cs}_2\text{AgBiBr}_6$, but also to change the nature from indirect to direct. This principle could be used to form either 2D/3D hybrid perovskites or quasi-2D perovskites to benefit from both the bandgap change of the 2D and the charge transport properties of the 3D compound. This might also lead to a change in the selectivity of the contacts because the energy levels of the 2D perovskite are changed due to the increase in the bandgap energy. Such approaches have been successfully realized for lead-halide perovskites; however, combining the benefits of both in a device is challenging.

Attempts of alloying or doping other elements into $\text{Cs}_2\text{AgBiBr}_6$ have been undertaken with the goal of reducing E_g . Some of these additives indeed influence the absorption onset (e.g., In and Sb,^[20,80] Rb,^[81] S^[82]) but most of them do not really shift it, meaning that E_g is not altered. Instead, the absorption becomes broader due to tail states, which helps to increase the current but is not beneficial for maintaining a high V_{oc} . Using the highly toxic element thallium, however, leads to an actual shift of the absorption onset and allowed for a decrease of E_g by 0.5 eV.^[83]

As already discussed above, disorder in the occupancy of the B-site is considered as a reason for the broad and redshifted PL. This effect could be exploited by intentionally generating disorder to reduce the bandgap as proposed early by first-principle calculations.^[84] An observed reduction of the single-crystal bandgap by 0.26 eV in a crystal engineering study was attributed to this effect.^[85] Enhanced order was also seen as reason for a slightly blueshifted absorption in single crystals for X-ray detectors.^[53] The role of temperature-induced bond length on the bandgap has also been discussed in the context of thermochromism.^[86]

Another promising approach for bismuth^[87] and nonbismuth double perovskites is the doping with Cu^{2+} ions which allows to reduce the bandgaps of several structures toward lower energies. A reduced bandgap has been reported for $\text{Cs}_2\text{AgSbCl}_6$ and $\text{Cs}_2\text{AgInCl}_6$ by 0.6–1.6 eV,^[88,89] although it seems here as well that a broad distribution of intragap states contributes to the shifted absorption onset.^[90]

To stay with the pure 3D double perovskites, a substitution of the elements opens up new opportunities. $\text{Cs}_2\text{NaFeCl}_6$ ^[91] (also doped with Ag^+ ions) or $\text{Cs}_2\text{AgFeCl}_6$ ^[92] exhibits reduced bandgap energies compared to $\text{Cs}_2\text{AgBiBr}_6$. However, other drawbacks, e.g., a low charge carrier mobility, can be found for these materials that have to be studied in order to overcome these problems. Also, the recently published $\text{Cu}_2\text{AgBiI}_6$ shows great potential with a direct bandgap with an energy of 2 eV.^[93]

Scientifically, the $\text{Cs}_2\text{AgBiBr}_6$ material remains highly interesting as its properties have not been completely understood neither from the chemistry nor the physics point of view. In terms of chemistry, the obvious differences of the optical properties of nominally the same material obtained by different synthesis methods are waiting for a unified explanation. In terms of physics, the rich absorption and emission (photoluminescence and EL) features remain of interest and their role in determining the solar cell efficiency, in particular the V_{oc} . Despite promising measurements on the diffusion length and mobility of charges, the low charge carrier collection efficiency remains an unresolved question, where the interplay between diffusion length, doping, the distribution of mobile ionic defects, and the properties of the contact materials has to be unraveled. In general, the role of mobile ions is only rudimentarily studied. Gaining deeper insights into the photophysics and especially the device physics of $\text{Cs}_2\text{AgBiBr}_6$ solar cells remains highly valuable, also considering promising novel related compounds such as the recently reported $\text{Cu}_2\text{AgBiI}_6$.^[93]

9. Conclusion

Altogether, we have to state that $\text{Cs}_2\text{AgBiBr}_6$ is not the ideal candidate for industrial solar cell applications. The high-temperature

annealing necessary for phase-pure synthesis, together with the unresolved question on achieving highest IQE, as well as the large and indirect bandgap raise too many obstacles to reach necessary efficiencies above 10%. Although several drawbacks can be overcome by device engineering, as well as hybridization of the dimension or optimization of the architecture, the only successful way to enhance the efficiency further would be changing the energy and/or the nature of the bandgap by the synthesis of, e.g., $\text{Cs}_2\text{AgBiI}_6$. However, $\text{Cs}_2\text{AgBiBr}_6$ remains a highly interesting material as it shows a big potential to be used in stable X-ray or photodetectors. Moreover, due to its unique chemical and physical properties, this material rises a lot of interests regarding the exploration of these and thus getting to know this class of materials throughout in order to synthesize and investigate new compounds. Also, getting to know the exact processes in solar cells comprising this material will be highly valuable to investigate other materials, especially because lead-free double perovskites behave rather differently compared to lead-based perovskites.

Supporting Information

Supporting Information is available from the Wiley Online Library or from the author.

Acknowledgements

W.T. acknowledges funding from the European Union's Horizon 2020 research and innovation program under grant agreement no. 851676 (ERC StGrt). M.T.S. acknowledges Prof. Thomas Bein from LMU for introduction to the double perovskites and the funding from the German Science Foundation (DFG) focus program SPP2169 and the DFG Excellence Cluster e-conversion (EXC 2089/1-390776260).

Open access funding enabled and organized by Projekt DEAL.

Conflict of Interest

The authors declare no conflict of interest.

Keywords

double perovskites, lead-free perovskites, photovoltaics, solar cells

Received: September 21, 2021

Revised: November 9, 2021

Published online:

- [1] W. Tress, *Adv. Energy Mater.* **2017**, *7*, 1602358.
- [2] J.-P. Correa-Baena, M. Saliba, T. Buonassisi, M. Grätzel, A. Abate, W. Tress, A. Hagfeldt, *Science* **2017**, *358*, 739.
- [3] P. Billen, E. Leccisi, S. Dastidar, S. Li, L. Lobaton, S. Spatarì, A. T. Fafarman, V. M. Fthenakis, J. B. Baxter, *Energy* **2019**, *166*, 1089.
- [4] M. Chen, M.-G. Ju, H. F. Garces, A. D. Carl, L. K. Ono, Z. Hawash, Y. Zhang, T. Shen, Y. Qi, R. L. Grimm, D. Pacifici, X. C. Zeng, Y. Zhou, N. P. Padture, *Nat. Commun.* **2019**, *10*, 16.
- [5] F. Hao, C. C. Stoumpos, D. H. Cao, R. P. H. Chang, M. G. Kanatzidis, *Nat. Photonics* **2014**, *8*, 489.
- [6] N. K. Noel, S. D. Stranks, A. Abate, C. Wehrenfennig, S. Guarnera, A.-A. Haghighirad, A. Sadhanala, G. E. Eperon, S. K. Pathak,

- M. B. Johnston, A. Petrozza, L. M. Herz, H. J. Snaith, *Energy Environ. Sci.* **2014**, *7*, 3061.
- [7] K. Nishimura, M. A. Kamarudin, D. Hirotsu, K. Hamada, Q. Shen, S. Iikubo, T. Minemoto, K. Yoshino, S. Hayase, *Nano Energy* **2020**, *74*, 104858.
- [8] F. Hao, C. C. Stoumpos, P. Guo, N. Zhou, T. J. Marks, R. P. H. Chang, M. G. Kanatzidis, *J. Am. Chem. Soc.* **2015**, *137*, 11445.
- [9] A. H. Slavney, T. Hu, A. M. Lindenberg, H. I. Karunadasa, *J. Am. Chem. Soc.* **2016**, *138*, 2138.
- [10] E. T. McClure, M. R. Ball, W. Windl, P. M. Woodward, *Chem. Mater.* **2016**, *28*, 1348.
- [11] W. Pan, H. Wu, J. Luo, Z. Deng, C. Ge, C. Chen, X. Jiang, W.-J. Yin, G. Niu, L. Zhu, L. Yin, Y. Zhou, Q. Xie, X. Ke, M. Sui, J. Tang, *Nat. Photonics* **2017**, *11*, 726.
- [12] M. Armer, J. Höcker, C. Büchner, S. Häfele, P. Dörflinger, M. Sirtl, K. Tvingstedt, T. Bein, V. Dyakonov, *CrystEngComm* **2021**.
- [13] E. Greul, M. L. Petrus, A. Binek, P. Docampo, T. Bein, *J. Mater. Chem. A* **2017**, *5*, 19972.
- [14] W. Gao, C. Ran, J. Xi, B. Jiao, W. Zhang, M. Wu, X. Hou, Z. Wu, *ChemPhysChem* **2018**, *19*, 1696.
- [15] F. Igbari, R. Wang, Z.-K. Wang, X.-J. Ma, Q. Wang, K.-L. Wang, Y. Zhang, L.-S. Liao, Y. Yang, *Nano Lett.* **2019**, *19*, 2066.
- [16] X. Yang, Y. Chen, P. Liu, H. Xiang, W. Wang, R. Ran, W. Zhou, Z. Shao, *Adv. Funct. Mater.* **2020**, *30*, 2001557.
- [17] H. Lei, D. Hardy, F. Gao, *Adv. Funct. Mater.* **2021**, 2105898.
- [18] Y. Wu, X. Li, H. Zeng, *Small Struct.* **2021**, *2*, 2000071.
- [19] X. Yang, W. Wang, R. Ran, W. Zhou, Z. Shao, *Energy Fuels* **2020**, *34*, 10513.
- [20] Z. Li, S. R. Kavanagh, M. Napari, R. G. Palgrave, M. Abdi-Jalebi, Z. Andaji-Garmaroudi, D. W. Davies, M. Laitinen, J. Julin, M. A. Isaacs, R. H. Friend, D. O. Scanlon, A. Walsh, R. L. Z. Hoyer, *J. Mater. Chem. A* **2020**, *8*, 21780.
- [21] C. N. Savory, A. Walsh, D. O. Scanlon, *ACS Energy Lett.* **2016**, *1*, 949.
- [22] L. Yu, A. Zunger, *Phys. Rev. Lett.* **2012**, *108*, 068701.
- [23] G. E. Eperon, S. D. Stranks, C. Menelaou, M. B. Johnston, L. M. Herz, H. J. Snaith, *Energy Environ. Sci.* **2014**, *7*, 982.
- [24] M. T. Sirtl, F. Ebad, B. T. van Gorkom, P. Ganswindt, R. A. J. Janssen, T. Bein, W. Tress, *Adv. Opt. Mater.* **2021**, *9*, 2100202.
- [25] W. Ning, F. Wang, B. Wu, J. Lu, Z. Yan, X. Liu, Y. Tao, J.-M. Liu, W. Huang, M. Fahlman, L. Hultman, T. C. Sum, F. Gao, *Adv. Mater.* **2018**, *30*, 1706246.
- [26] M. T. Sirtl, M. Armer, L. K. Reb, R. Hooijer, P. Dörflinger, M. A. Scheel, K. Tvingstedt, P. Rieder, N. Glück, P. Pandit, S. V. Roth, P. Müller-Buschbaum, V. Dyakonov, T. Bein, *ACS Appl. Energy Mater.* **2020**.
- [27] R. L. Z. Hoyer, L. Eyre, F. Wei, F. Brivio, A. Sadhanala, S. Sun, W. Li, K. H. L. Zhang, J. L. MacManus-Driscoll, P. D. Bristowe, R. H. Friend, A. K. Cheetham, F. Deschler, *Adv. Mater. Interfaces* **2018**, *5*, 1800464.
- [28] G. Longo, S. Mahesh, L. R. V. Buizza, A. D. Wright, A. J. Ramadan, M. Abdi-Jalebi, P. K. Nayak, L. M. Herz, H. J. Snaith, *ACS Energy Lett.* **2020**, *5*, 2200.
- [29] U. Rau, *Phys. Rev. B* **2007**, *76*, 085303.
- [30] J. Yang, P. Zhang, S.-H. Wei, *J. Phys. Chem. Lett.* **2018**, *9*, 31.
- [31] J. A. Steele, P. Puech, M. Keshavarz, R. Yang, S. Banerjee, E. Debroye, C. W. Kim, H. Yuan, N. H. Heo, J. Vanacken, A. Walsh, J. Hofkens, M. B. J. Roeffaers, *ACS Nano* **2018**, *12*, 8081.
- [32] R. Kentsch, M. Scholz, J. Horn, D. Schlettwein, K. Oum, T. Lenzer, *J. Phys. Chem. C* **2018**, *122*, 25940.
- [33] S. J. Zelewski, J. M. Urban, A. Surrante, D. K. Maude, A. Kuc, L. Schade, R. D. Johnson, M. Dollmann, P. K. Nayak, H. J. Snaith, P. Radaelli, R. Kudrawiec, R. J. Nicholas, P. Plochocka, M. Baranowski, *J. Mater. Chem. C* **2019**, *7*, 8350.
- [34] B. Yang, J. Chen, S. Yang, F. Hong, L. Sun, P. Han, T. Pullerits, W. Deng, K. Han, *Angew. Chem. Int. Ed.* **2018**, *57*, 5359.
- [35] M. R. Filip, S. Hillman, A. A. Haghighirad, H. J. Snaith, F. Giustino, *J. Phys. Chem. Lett.* **2016**, *7*, 2579.
- [36] Q. Lin, A. Armin, R. C. R. Nagiri, P. L. Burn, P. Meredith, *Nat. Photonics* **2015**, *9*, 106.
- [37] A. Schmitz, L. L. Schaberg, S. Sirovinskaya, M. Pantaler, D. C. Lupascu, N. Benson, G. Bacher, *ACS Energy Lett.* **2020**, *5*, 559.
- [38] Y. Bekenstein, J. C. Dahl, J. Huang, W. T. Osowiecki, J. K. Swabeck, E. M. Chan, P. Yang, A. P. Alivisatos, *Nano Lett.* **2018**, *18*, 3502.
- [39] L. Schade, A. D. Wright, R. D. Johnson, M. Dollmann, B. Wenger, P. K. Nayak, D. Prabhakaran, L. M. Herz, R. Nicholas, H. J. Snaith, P. G. Radaelli, *ACS Energy Lett.* **2019**, *4*, 299.
- [40] B. Wang, L. Yang, C. Dall'Agnese, A. K. Jena, S. Sasaki, T. Miyasaka, H. Tamiaki, X.-F. Wang, *Sol. RRL* **2020**, *4*, 2000166.
- [41] M. Delor, A. H. Slavney, N. R. Wolf, M. R. Filip, J. B. Neaton, H. I. Karunadasa, N. S. Ginsberg, *ACS Energy Lett.* **2020**, *5*, 1337.
- [42] D. Bartesaghi, A. H. Slavney, M. C. Gélvez-Rueda, B. A. Connor, F. C. Grozema, H. I. Karunadasa, T. J. Savenije, *J. Phys. Chem. C* **2018**, *122*, 4809.
- [43] E. M. Hutter, M. C. Gélvez-Rueda, D. Bartesaghi, F. C. Grozema, T. J. Savenije, *ACS Omega* **2018**, *3*, 11655.
- [44] A. D. Wright, L. R. V. Buizza, K. J. Savill, G. Longo, H. J. Snaith, M. B. Johnston, L. M. Herz, *J. Phys. Chem. Lett.* **2021**, *12*, 3352.
- [45] J. Xiu, Y. Shao, L. Chen, Y. Feng, J. Dai, X. Zhang, Y. Lin, Y. Zhu, Z. Wu, Y. Zheng, H. Pan, C. Liu, X. Shi, X. Cheng, Z. He, *Mater. Today Energy* **2019**, *12*, 186.
- [46] M. Pantaler, K. T. Cho, V. I. E. Queloz, I. García Benito, C. Fettkenhauer, I. Anusca, M. K. Nazeeruddin, D. C. Lupascu, G. Grancini, *ACS Energy Lett.* **2018**, *3*, 1781.
- [47] W. Tress, *J. Phys. Chem. Lett.* **2017**, *8*, 3106.
- [48] M. Ghasemi, L. Zhang, J.-H. Yun, M. Hao, D. He, P. Chen, Y. Bai, T. Lin, M. Xiao, A. Du, M. Lyu, L. Wang, *Adv. Funct. Mater.* **2020**, *30*, 2002342.
- [49] M. F. Aygüler, A. G. Hufnagel, P. Rieder, M. Wussler, W. Jaegermann, T. Bein, V. Dyakonov, M. L. Petrus, A. Baumann, P. Docampo, *ACS Appl. Mater. Interfaces* **2018**, *10*, 11414.
- [50] L. Yin, H. Wu, W. Pan, B. Yang, P. Li, J. Luo, G. Niu, J. Tang, *Adv. Opt. Mater.* **2019**, *7*, 1900491.
- [51] J. A. Steele, W. Pan, C. Martin, M. Keshavarz, E. Debroye, H. Yuan, S. Banerjee, E. Fron, D. Jonckheere, C. W. Kim, W. Baekelant, G. Niu, J. Tang, J. Vanacken, M. V. der Auweraer, J. Hofkens, M. B. J. Roeffaers, *Adv. Mater.* **2018**, *30*, 1804450.
- [52] H. Chen, C. Wu, R. Li, H. Chen, *Crystals* **2021**, *11*, 1101.
- [53] W. Yuan, G. Niu, Y. Xian, H. Wu, H. Wang, H. Yin, P. Liu, W. Li, J. Fan, *Adv. Funct. Mater.* **2019**, *29*, 1900234.
- [54] C. Wu, Q. Zhang, Y. Liu, W. Luo, X. Guo, Z. Huang, H. Ting, W. Sun, X. Zhong, S. Wei, S. Wang, Z. Chen, L. Xiao, *Adv. Sci.* **2018**, *5*, 1700759.
- [55] N. Rodkey, S. Kaal, P. Sebastia-Luna, Y. A. Birkhölzer, M. Ledinsky, F. Palazon, H. J. Bolink, M. Morales-Masis, *Chem. Mater.* **2021**, *33*, 7417.
- [56] N. Daem, J. Dewalque, F. Lang, A. Maho, G. Spronck, C. Henrict, P. Colson, S. D. Stranks, R. Cloots, *Sol. RRL* **2021**, *5*, 2100422.
- [57] X. Zhang, X. Liu, B. Sun, H. Ye, C. He, L. Kong, G. Li, Z. Liu, G. Liao, *ACS Appl. Mater. Interfaces* **2021**, *13*, 35949.
- [58] M. Wang, P. Zeng, S. Bai, J. Gu, F. Li, Z. Yang, M. Liu, *Sol. RRL* **2018**, *2*, 1800217.
- [59] P. Fan, H.-X. Peng, Z.-H. Zheng, Z.-H. Chen, S.-J. Tan, X.-Y. Chen, Y.-D. Luo, Z.-H. Su, J.-T. Luo, G.-X. Liang, *Nanomaterials* **2019**, *9*, 1760.
- [60] A. D. Taylor, Q. Sun, K. P. Goetz, Q. An, T. Schramm, Y. Hofstetter, M. Litterst, F. Paulus, Y. Vaynzof, *Nat. Commun.* **2021**, *12*, 1878.

- [61] M. S. Shadabroo, H. Abdizadeh, M. R. Golobostanfard, *ACS Appl. Energy Mater.* **2021**, *4*, 6797.
- [62] X. Yang, A. Xie, H. Xiang, W. Wang, R. Ran, W. Zhou, Z. Shao, *Appl. Phys. Rev.* **2021**, *8*, 041402.
- [63] A. Maiti, A. J. Pal, *J. Phys. Chem. C* **2021**, *125*, 16324.
- [64] B. Xiao, Y. Tan, Z. Yi, Y. Luo, Q. Jiang, J. Yang, *ACS Appl. Mater. Interfaces* **2021**, *13*, 37027.
- [65] Z. Xiao, W. Meng, J. Wang, Y. Yan, *ChemSusChem* **2016**, *9*, 2628.
- [66] T. Li, X. Zhao, D. Yang, M.-H. Du, L. Zhang, *Phys. Rev. Appl.* **2018**, *10*, 041001.
- [67] B. Wang, N. Li, L. Yang, C. Dall'Agnese, A. K. Jena, T. Miyasaka, X.-F. Wang, *J. Am. Chem. Soc.* **2021**.
- [68] S. Yin, Y. Cheng, Y. Li, W. Liang, T. Li, J. Ma, D. Wu, Z. Shi, X. Li, *J. Mater. Sci.* **2021**, *56*, 13633.
- [69] Y. Li, Z. Shi, L. Lei, S. Li, D. Yang, D. Wu, T. Xu, Y. Tian, Y. Lu, Y. Wang, L. Zhang, X. Li, Y. Zhang, G. Du, C. Shan, *Adv. Mater. Interfaces* **2019**, *6*, 1900188.
- [70] L.-Z. Lei, Z.-F. Shi, Y. Li, Z.-Z. Ma, F. Zhang, T.-T. Xu, Y.-T. Tian, D. Wu, X.-J. Li, G.-T. Du, *J. Mater. Chem. C* **2018**, *6*, 7982.
- [71] J. Yang, C. Bao, W. Ning, B. Wu, F. Ji, Z. Yan, Y. Tao, J.-M. Liu, T. C. Sum, S. Bai, J. Wang, W. Huang, W. Zhang, F. Gao, *Adv. Opt. Mater.* **2019**, *7*, 1801732.
- [72] M. Wang, P. Zeng, Z. Wang, M. Liu, *Adv. Sci.* **2020**, *7*, 1903662.
- [73] P. Vishnoi, R. Seshadri, A. K. Cheetham, *J. Phys. Chem. C* **2021**, *125*, 11756.
- [74] B. Ghosh, B. Wu, H. K. Mulmudi, C. Guet, K. Weber, T. C. Sum, S. Mhaisalkar, N. Mathews, *ACS Appl. Mater. Interfaces* **2018**, *10*, 35000.
- [75] S. E. Creutz, E. N. Crites, M. C. De Siena, D. R. Gamelin, *Nano Lett.* **2018**, *18*, 1118.
- [76] D. Wu, X. Zhao, Y. Huang, J. Lai, H. Li, J. Yang, C. Tian, P. He, Q. Huang, X. Tang, *Chem. Mater.* **2021**, *33*, 4971.
- [77] M. K. Jana, S. M. Janke, D. J. Dirkes, S. Dovletgeldi, C. Liu, X. Qin, K. Gundogdu, W. You, V. Blum, D. B. Mitzi, *J. Am. Chem. Soc.* **2019**, *141*, 7955.
- [78] Y. Yao, B. Kou, Y. Peng, Z. Wu, L. Li, S. Wang, X. Zhang, X. Liu, J. Luo, *Chem. Commun.* **2020**, *56*, 3206.
- [79] L.-Y. Bi, Y.-Q. Hu, M.-Q. Li, T.-L. Hu, H.-L. Zhang, X.-T. Yin, W.-X. Que, M. S. Lassoued, Y.-Z. Zheng, *J. Mater. Chem. A* **2019**, *7*, 19662.
- [80] K. Du, W. Meng, X. Wang, Y. Yan, D. B. Mitzi, *Angew. Chem. Int. Ed.* **2017**, *56*, 8158.
- [81] Z. Zhang, C. Wu, D. Wang, G. Liu, Q. Zhang, W. Luo, X. Qi, X. Guo, Y. Zhang, Y. Lao, B. Qu, L. Xiao, Z. Chen, *Org. Electron.* **2019**, *74*, 204.
- [82] N. Pai, J. Lu, M. Wang, A. S. R. Chesman, A. Seeber, P. V. Cherepanov, D. C. Senevirathna, T. R. Gengenbach, N. V. Medhekar, P. C. Andrews, U. Bach, A. N. Simonov, *J. Mater. Chem. A* **2020**, *8*, 2008.
- [83] A. H. Slavney, L. Leppert, D. Bartesaghi, A. Gold-Parker, M. F. Toney, T. J. Savenije, J. B. Neaton, H. I. Karunadasa, *J. Am. Chem. Soc.* **2017**, *139*, 5015.
- [84] X.-G. Zhao, J.-H. Yang, Y. Fu, D. Yang, Q. Xu, L. Yu, S.-H. Wei, L. Zhang, *J. Am. Chem. Soc.* **2017**, *139*, 2630.
- [85] F. Ji, J. Klarbring, F. Wang, W. Ning, L. Wang, C. Yin, J. S. M. Figueroa, C. K. Christensen, M. Etter, T. Ederth, L. Sun, S. I. Simak, I. A. Abrikosov, F. Gao, *Angew. Chem. Int. Ed.* **2020**, *59*, 15191.
- [86] W. Ning, X.-G. Zhao, J. Klarbring, S. Bai, F. Ji, F. Wang, S. I. Simak, Y. Tao, X.-M. Ren, L. Zhang, W. Huang, I. A. Abrikosov, F. Gao, *Adv. Funct. Mater.* **2019**, *29*, 1807375.
- [87] F. Ji, Y. Huang, F. Wang, L. Kobera, F. Xie, J. Klarbring, S. Abbrent, J. Brus, C. Yin, S. I. Simak, I. A. Abrikosov, I. A. Buyanova, W. M. Chen, F. Gao, *Adv. Funct. Mater.* **2020**, *30*, 2005521.
- [88] A. Karmakar, M. S. Dodd, S. Agnihotri, E. Ravera, V. K. Michaelis, *Chem. Mater.* **2018**, *30*, 8280.
- [89] Q. Liao, J. Chen, L. Zhou, T. Wei, L. Zhang, D. Chen, F. Huang, Q. Pang, J. Z. Zhang, *J. Phys. Chem. Lett.* **2020**, *11*, 8392.
- [90] T. Appadurai, S. Chaure, M. Mala, A. K. Chandiran, *Energy Fuels* **2021**, *35*, 11479.
- [91] Y. Xian, H. Yin, Y. Bao, Y. Xiao, S. Yuan, N. U. Rahman, Y. Yuan, Y. Zhang, X. Meng, S. Jin, W. Li, J. Fan, *J. Phys. Chem. Lett.* **2020**, *11*, 9535.
- [92] H. Yin, Y. Xian, Y. Zhang, W. Chen, X. Wen, N. U. Rahman, Y. Long, B. Jia, J. Fan, W. Li, *Adv. Funct. Mater.* **2020**, *30*, 2002225.
- [93] H. C. Sansom, G. Longo, A. D. Wright, L. R. V. Buizza, S. Mahesh, B. Wenger, M. Zanella, M. Abdi-Jalebi, M. J. Pitcher, M. S. Dyer, T. D. Manning, R. H. Friend, L. M. Herz, H. J. Snaith, J. B. Claridge, M. J. Rosseinsky, *J. Am. Chem. Soc.* **2021**, *143*, 3983.



Wolfgang Tress is currently a senior lecturer at Zurich University of Applied Sciences (ZHAW) leading the ERC-funded novel semiconductor devices group. His interests include characterizing and modeling of novel semiconductor materials and photovoltaic devices. Recently, he has been working on the device physics and the mixed ionic–electronic conductivity of perovskites. Prior to his appointment at ZHAW, he was an Ambizione fellow at the Graetzel and Hagfeldt labs at EPFL and a Marie Curie fellow at LMU. Based on his Ph.D. thesis at TU Dresden and postdoctoral research in the Inganäs group, he published a monograph on organic solar cells.



Maximilian Sirtl received his Ph.D. degree in physical chemistry from the Department of Chemistry at the University of Munich (LMU), Germany. During his Ph.D. studies, supervised by Professor Thomas Bein, he focused on the synthesis and investigation of both pristine thin films and complete solar cells comprising $\text{Cs}_2\text{AgBiBr}_6$. He moreover worked on different hole-transporting materials to study the influence on the performance both on lead-based and lead-free perovskite solar cells. Continuing his work, he investigates the bottlenecks of $\text{Cs}_2\text{AgBiBr}_6$ and works on possibilities to improve the overall performance of solar cells based on this material.